


Please cite the Published Version

Liu, Y, Fan, Z, Yu, S, Zhang, R, Zhang, J, Liskiewicz, TW , Ge, X and Wang, W (2024) Macroscale structural superlubricity: Dynamic evolution of tribolayers in two-dimensional materials under extreme pressure. Nano Energy, 129. 110072 ISSN 2211-2855

DOI: <https://doi.org/10.1016/j.nanoen.2024.110072>

Publisher: Elsevier

Version: Accepted Version

Downloaded from: <https://e-space.mmu.ac.uk/635281/>

Usage rights:  [Creative Commons: Attribution 4.0](https://creativecommons.org/licenses/by/4.0/)

Additional Information: This is an author accepted manuscript of an article published in Nano Energy, by Elsevier.

Enquiries:

If you have questions about this document, contact openresearch@mmu.ac.uk. Please include the URL of the record in e-space. If you believe that your, or a third party's rights have been compromised through this document please see our Take Down policy (available from <https://www.mmu.ac.uk/library/using-the-library/policies-and-guidelines>)

Macroscale Structural Superlubricity: Dynamic Evolution of Tribolayers in Two-Dimensional Materials Under Extreme Pressure

*Yanfei Liu^{*1}, Zhikai Fan¹, Shengtao Yu¹, Ruize Zhang¹, Jie Zhang², Tomasz W. Liskiewicz³, Xiangyu Ge¹, Wenzhong Wang¹*

¹ *School of Mechanical Engineering, Beijing Institute of Technology, Beijing, 100081, China*

² *School of Mechanical Engineering, University of Science and Technology Beijing, Beijing, 100083, China*

³ *Department of Engineering, Faculty of Science and Engineering, Manchester Metropolitan University, Manchester M1 5GD, UK*

*Corresponding author. **E-mail:** liuyanfei@bit.edu.cn (Yanfei Liu)

Tel: 8610- 68912719.

Abstract

Achieving macroscale structural superlubricity with two-dimensional (2D) materials under ultrahigh contact pressure in ambient condition is particularly challenging. Furthermore, the mechanisms underlying the disparate trans-scale tribological behaviors of 2D materials continue to be a subject of debate. Here, we propose a novel principle concerning pressure-induced dynamic structural evolution and tribochemical behaviors of tribolayers to broaden the macroscale structural superlubricity. For the first time, robust macroscale structural superlubricity with ultralow wear rate is realized by 2D material coating in ambient condition by sliding steel counterparts under ultrahigh contact pressure. The results reveal that macroscale structural superlubricity of 2D materials is highly dependent on the dynamic evolution of tribolayers nanostructures, as well as the adsorption and tribochemical behaviors governed by extreme pressure. These findings shed light on achieving robust macroscale structural superlubricity with 2D materials for harsh engineering conditions.

Keywords: Macroscale structural superlubricity; 2D materials; Ambient condition; Ultrahigh contact pressure

1. Introduction

Industrial production typically involves a significant degree of energy consumption and economic losses due to friction and wear [1]. Lubricants are widely used in engineering applications to enhance the economic efficiency and service life of machines. However, conventional lubricants do not meet the requirements of extreme environments, including high vacuum and alternating high/low temperatures. Therefore, solid lubricants have been developed for tribological applications in harsh environments. For instance, coating materials such as MoS₂ [2, 3], diamond-like carbon [4-7], and nanocomposites coatings [8, 9] are widely used in mechanical systems. Recently, the tribological behaviors of two-dimensional (2D) materials, including transition metal dichalcogenides [10-12], hexagonal boron nitride [13], graphene family materials [14-18], and MXenes [19-23], have been widely evaluated owing to the ease of slippage between the lattice layers, which are considered as a promising solution to reduce friction and wear in real mechanical systems.[24, 25]

Superlubricity, referring to a lubrication state with virtually vanished friction (typically defined as a coefficient of friction (COF) lower than 0.01), has attracted significant attention from researchers. In 1990, Hirano and Shinjo [26] proposed the relationship between friction and atomic locking. Structural superlubricity state achieved by incommensurate contact was firstly theoretically predicted. In the subsequent studies, it was proved that the superlubricity can be achieved by 2D materials [27, 28] or heterojunctions [13, 29]. Among layered 2D materials, graphene family materials

exhibit superior properties, including high thermal conductivity, high tensile strength, and high chemical stability. Previous studies have found that a significant reduction in the COF can be achieved even with single-layer pristine graphene (PG) lubrication. [30] In recent years, it has been reported that the superlubricity state can be realized at the nano [31] and micro scales (usually with normal load in the orders of nN and μN) [32] using graphene as a solid lubricant, which can be ascribed to the atomically flat surface, low surface energy, and incommensurate contact between the lattice layers, facilitating interlayer slippage. However, the macroscale COF with graphene family solid lubricants is typically significantly higher than the nanoscale or microscale [33, 34]. The structural imperfections at the sliding interface, disordering, puckering, and edge effects of graphene nanoflakes can lead to additional energy dissipation during friction.[35] Besides graphene family materials, transition metal dichalcogenides (TMDs) are widely used 2D materials as solid lubricants for vacuum conditions or inert gas atmospheres [36]. Structural superlubricity can be also realized by sliding between MoS_2 nanoflakes at the nanoscale [37]. Structural superlubricity can be achieved by both the graphene family materials and TMDs at the nanoscale or microscale. However, the tribological behaviors of these 2D materials exhibit significant differences at the macroscale, where the underlying mechanisms for the mismatched trans-scale tribological behaviors are not well understood.

For nanoscale/microscale tribological experiments, the structure of the sliding interface can be precisely controlled. However, the dynamic evolution of the interfacial structure

under varied contact pressures is highly related to the macroscale tribological behaviors. Currently, there is a lack of systematic investigation into the diverse dynamic structural evolution of 2D materials as solid lubricants, resulting in an inadequate understanding of the varied macroscale tribological properties of these materials. Recognizing the influence of dynamic interfacial structural evolution on the macroscale tribological behaviors of 2D materials under varied contact pressures holds significant importance for engineering applications and scientific research.

Here, for the first time, we report a robust macroscale structural superlubricity with 2D materials as solid lubricants by sliding steel counterparts under ultrahigh contact pressure of up to ~ 3.55 GPa. Macroscale tribological behaviors of commonly used 2D materials including graphene family materials (PG, graphene oxide (GO), fluorinated graphene (FG)), and TMDs (MoS_2 and WS_2) were tested under a wide of applied normal loads. Detailed characterizations were conducted on the sliding contact surfaces to understand the tribo-induced interfacial chemical and physical evolution under different contact pressures and its influence on the macroscale tribological behaviors. Our findings offer fundamental insights into the lubrication mechanisms of 2D materials as solid lubricants under varied contact pressure, promoting their potential engineering applications as solid lubricants.

2. Results

2.1 Solid lubrication and wear reduction behaviors

2.1.1 Comparison of graphene family coatings

The coatings were deposited onto engineering steel plates (details in the “Coating preparation and characterization” section in Supporting Information) to investigate the interfacial structural evolution and its impact on the macroscale solid lubrication and wear reduction properties under a wide range of contact pressures (Fig. 1a). The 2D materials used in this study can be mainly categorized as graphene family materials and TMDs (Figs. S1 and S2). Hence, the properties of these two groups of materials are presented separately, which makes the results more comparable, thus promoting the understanding of the different tribological behaviors and the underlying mechanisms of 2D materials as solid lubricants.

The functionalization and contact pressure dependences of solid lubrication and wear reduction behaviors of the graphene coatings (Fig. S3) were firstly evaluated by friction tests under ambient condition ($30\pm 1^\circ\text{C}$; relative humidity of $40\pm 10\%$) against 9.525 mm engineering steel balls as counterparts (Fig. S4). Interestingly, the graphene coatings exhibited different responses to applied normal loads. Figures 1b and 1c show the COF obtained in the tests using the deposited PG coating as a lubricant under different normal loads. The average COF of PG coating at a normal load of 2 N was 0.102. The average COF slightly decreased to 0.090 at a load of 10 N and then slightly increased to 0.107 at a load of 100 N. When the normal load was increased to 200 N,

the COF clearly rose during the friction test. The average steady-state COF of 0.259 was also higher than that at lower normal loads. We also found that stable lubrication cannot be realized with PG coating under a normal load of 400 N. These results indicate that the PG coating cannot provide sufficient lubrication under high normal loads.

For GO and FG coatings, the COFs decreased with an increase in the normal load. The average COFs of the GO coatings (Figs. 1d and 1e) were 0.153, 0.140, 0.133, 0.126, and 0.097 at normal loads of 2 N, 10 N, 100 N, 200 N, and 400 N, respectively. For GO coating, the COF at 400 N was 36.60% lower than that at 2 N. For FG coating (Figs. 1f and 1g), the average COFs at normal loads of 2 N, 10 N, 100 N, 200 N, and 400 N were 0.120, 0.084, 0.055, 0.048, and 0.041, respectively. FG coating also provided better lubrication at a high normal load of 400 N, which mainly resulted in a 65.83% reduction in the COF compared with that at a normal load of 2 N; furthermore, the COF was more stable during the friction process (Fig. 1f). These results highlight the excellent lubrication performance of FG coating as a solid lubricant, particularly at extremely high normal loads. The lubrication lifetimes of the three coatings were also evaluated at low and high normal loads (Fig. S5). At a low normal load of 2 N, PG coating could only provide lubrication for approximately 2,500 s, whereas GO and FG coatings could provide lubrication for over 18,000 s. For lubrication by FG coating at a normal load of 2 N, the COF slightly decreased after the initial 6,000 s friction process and a stable lubrication state was maintained with an average COF of approximately 0.098. At a high normal load, FG coating exhibited a longer lubrication lifetime than PG and GO

coatings, where the fluctuation of COF with FG coating can be attributed to the dynamic removal and formation of tribolayers. The lubricating behavior of the graphene coatings showed distinctly different responses to changes in the normal load. Among the three solid lubricant coatings with different graphene nanoflakes, FG coating exhibited the best lubrication performance, particularly at ultrahigh contact pressures.

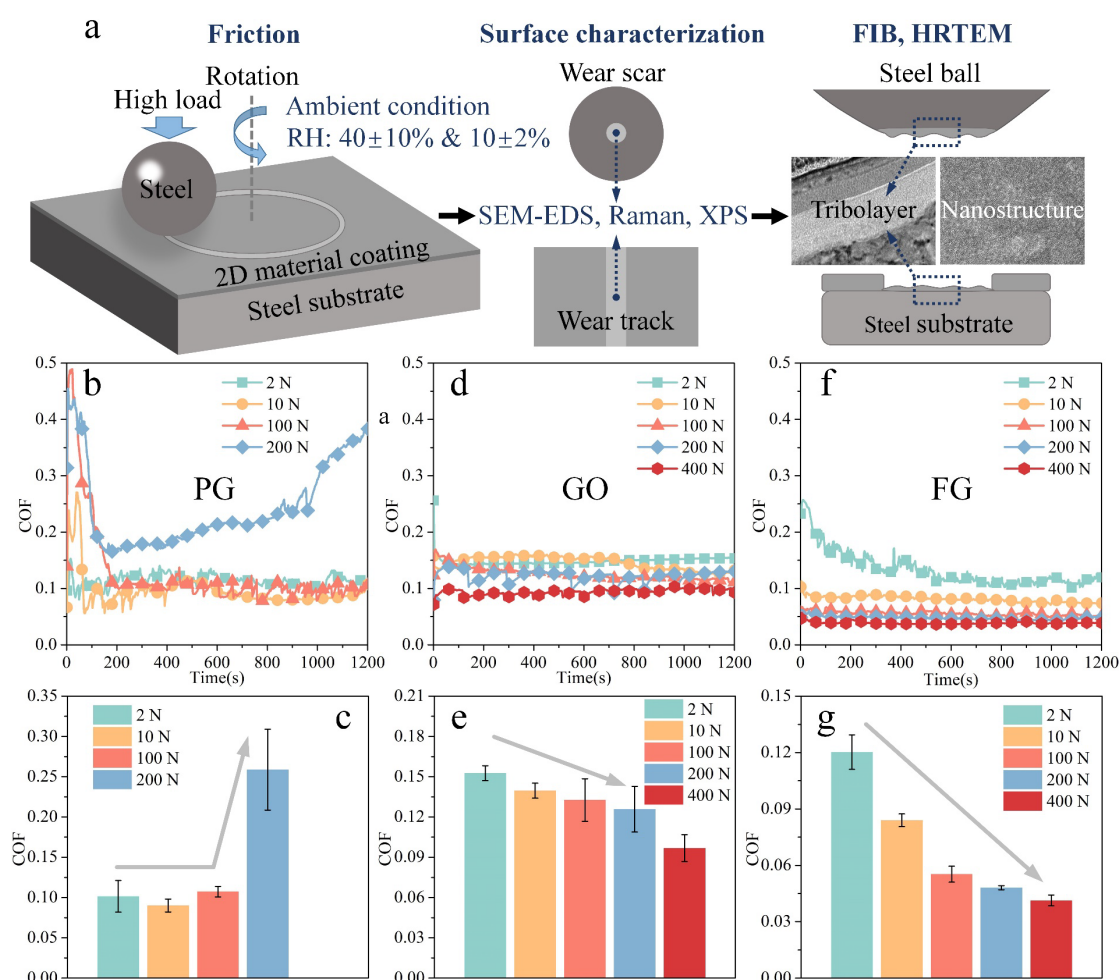


Figure 1. Schematic of the experimental setup (a), and the macroscale lubrication behaviors of graphene coatings under varied normal loads (30±1 °C; relative humidity of 40±10%; 12.56 mm/s). Variations in the COF and average steady-state COFs for steel substrates covered with (b, c) PG coatings, (d, e) GO coatings, and (f, g) FG coatings at different normal loads. The COF decreases with an increase in the normal load for lubrication by GO and FG coatings. The error bars represent the standard deviations. FG coating as a solid lubricant had the lowest COF at high normal loads among the graphene coatings.

After determining the solid lubrication behaviors of the graphene coatings at different normal loads, the features of the contact surfaces were analyzed. The optical images, three-dimensional (3D) morphologies, and the wear rates (Fig. S6) of counterparts after friction tests at loads of 2 N and 100 N were obtained to evaluate the antiwear behavior of the graphene coatings at low and high normal loads, respectively. During the friction test at 2 N (Figs. S7 and S8), transfer layers formed on the wear scars of the counterpart steel balls, and tribofilms developed on the wear tracks on the steel substrates with lubrication by PG, GO, and FG coatings, providing protection. This made it difficult to observe the wear of both counterparts (Figs. S6 and S7). In contrast, the graphene coatings exhibited different wear resistance behaviors at high normal loads (Figs. S6, S9, and S10).

For PG coating at 100 N, the steel ball (Fig. S9a) and steel substrate (Figs. S9d and S9g) exhibited severe wear, indicating the limited wear resistance of the PG coating at a high normal load. However, for GO coating at 100 N, the wear of the steel substrate was hard to observed (Figs. S9e and S9h), which can be ascribed to the protection of the tribofilm comprising GO nanoflakes. For FG coating, only a slight wear (depth of 0.114 μm) was observed (Figs. S9f and S9i). The wear of the steel balls was also significantly suppressed by the GO and FG coatings, which were reduced by 99.44% and 98.35%, respectively compared with that of lubrication by PG coating (Figs. S6 and S9a–S9c). The relatively poor lubrication performance at high normal loads is one of the most significant shortcomings of graphene family materials as solid lubricants

[38], which largely limits their engineering applications. Our results indicate that FG coating, even when deposited using a simple drip casting method, can overcome this limitation. Excellent tribological behaviors with a superlow friction coefficient (COF of ~ 0.041) can be obtained at a normal load of 400 N (maximum contact pressure of 3.55 GPa based on Hertz contact theory).

2.1.2 Macroscale structural superlubricity achieved by TMDs coatings

In addition to graphene family materials, the lubrication behaviors of TMDs have also garnered significant attention in recent years [39-41]. For 2D materials as solid lubricants, environmental humidity has a significant on macroscale tribological properties. Pristine graphene exhibits better lubrication and wear resistance behaviors under relatively high humidity [42], while TMDs exhibit lower COF and longer lubrication lifetime under vacuum/inert gas conditions without water molecules [43-45]. We firstly conducted the macroscale friction tests of MoS₂ coating at 100 N under relative humidity of 40%. The results indicate that the MoS₂ coating failed to provide stable lubrication under such test conditions (Fig. S11). To better elucidate the contact pressure dependences of solid lubrication and wear reduction behaviors of the TMDs coatings, a lower relative humidity of $10 \pm 2\%$ was chosen for the friction tests.

The COF versus time curves, with the lubrication of the WS₂ coating, exhibit significant fluctuation during the 1200 s friction tests under varied normal loads (Fig. 2a). The average steady-state COF with the lubrication of WS₂ coatings at normal loads of 2 N, 10 N, 100 N, 200 N and 400 N were 0.134, 0.046, 0.018, 0.013, and 0.010, respectively

(Fig. 2b). In contrast, MoS₂ coatings exhibited a more stable lubrication performance (Fig. 2c). The average steady-state COF with the lubrication of MoS₂ coatings at normal loads of 2 N, 10 N, 100 N, 200 N and 400 N were 0.095, 0.046, 0.010, 0.007, and 0.004, respectively (Fig. 2d). For both, the WS₂ and MoS₂ coatings, the COF decreased with an increase in the normal load. Superlubricity can be achieved with the WS₂ coating under a high normal load of 400 N, whereas with the MoS₂ coating it can be attained at normal loads exceeding 100 N. Long duration friction test was also conducted for MoS₂ coating under a normal load of 400 N, showing that the stable macroscale structural superlubricity can be maintained for more than 15,000 s (Fig. 2e).

The wear rates (Fig. S12) of counterparts after friction tests for MoS₂ coatings at loads of 2 N and 400 N were obtained to evaluate the antiwear behavior. Under a high normal load of 400 N, a low wear rate of $1.20 \times 10^{-9} \text{ mm}^3/(\text{N}\cdot\text{m})$ was measured. The 3D morphology (Fig. S13) and optical images (Fig. S14) reveal that tribolayers can be formed on the counterpart surfaces under both low and high normal loads (2 N and 400 N, respectively). This formation of tribolayers successfully prevents direct contact between asperities, resulting in significantly suppressed wear.

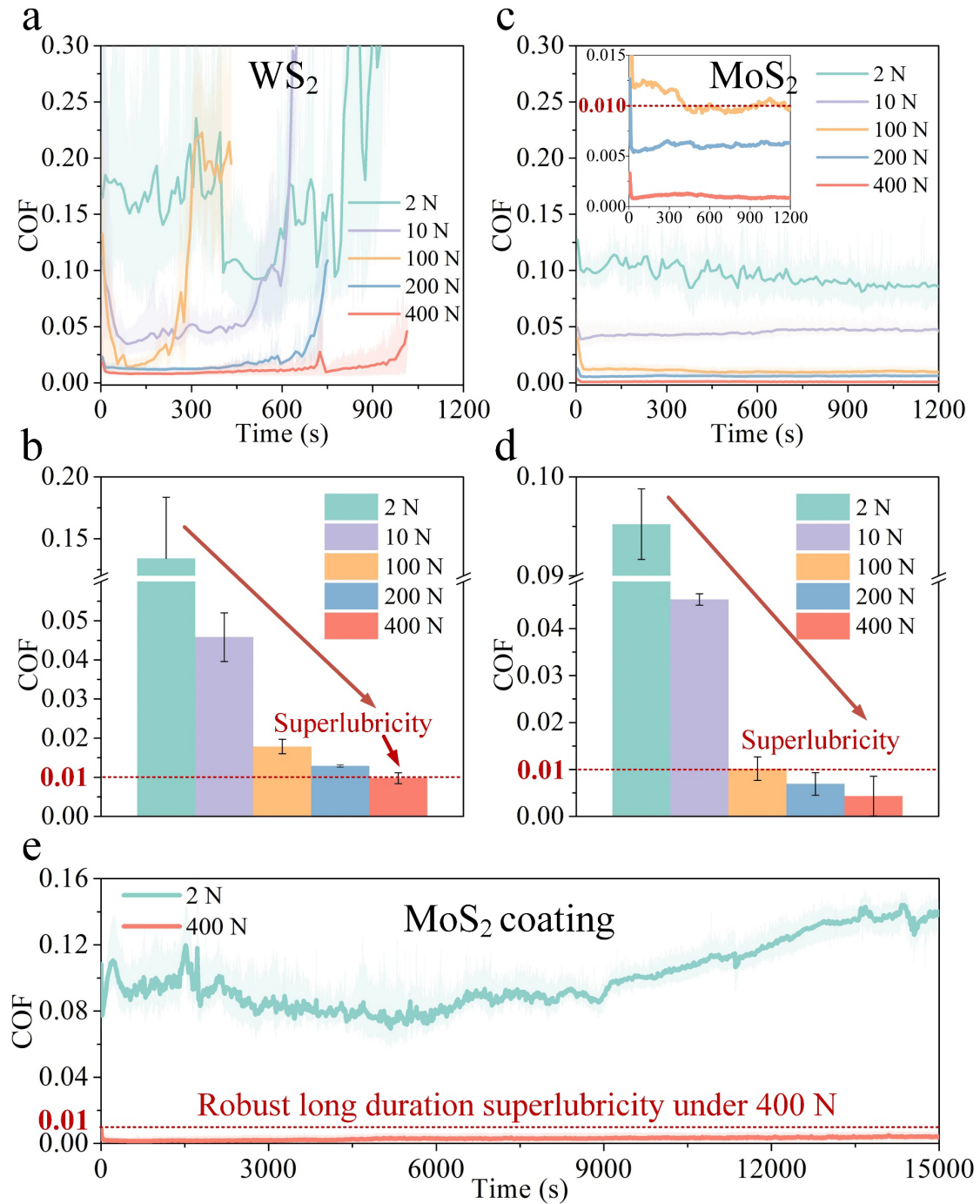


Figure 2. Macroscale lubrication behaviors of TMDs coatings under varied normal loads ($24\pm 1^\circ\text{C}$; relative humidity of $10\pm 2\%$; 12.56 mm/s). Variations in the COF for steel substrates covered with (a, b) WS₂ coatings and (c, d) MoS₂ coatings at different normal loads. The COF decreases as the normal load increases when lubricated with WS₂ and MoS₂ coatings. Average steady-state COFs were obtained from independent friction tests, where the error bars represent the standard deviations. Macroscale structural superlubricity can be achieved by WS₂ and MoS₂ coatings. (e) Robust superlubricity under ambient condition can be realized with the lubrication of MoS₂ coating for longer than 15,000 s.

2.2 Tribolayer formation

To further elucidate the underlying mechanisms behind the different friction phenomenon of solid lubrication coatings, state-of-art surface and interfacial characterization techniques were used to investigate the chemical and structural evolution of sliding contact surface induced by rubbing, thus to reveal the intrinsic correlation between the interfacial structure and macroscopic solid lubrication behaviors. It is well accepted that the tribolayers formed during friction play a critical role in solid lubrication processes. Therefore, the morphology and chemical composition of the contact surfaces of the counterparts in the friction tests were initially characterized to examine the formation of tribolayers with different solid lubricant coatings under varied contact pressures.

2.2.1 Pristine graphene coating

Initially, the friction-induced physical and chemical changes in the contact surfaces for the PG coating were examined. After the tests at 2 N, the transfer layer can be detected on the wear scar of the steel ball from the scanning electron microscope (SEM) image (Fig. 3a). The energy dispersive spectrometer (EDS) mapping results (Figs. 3a1–3a3) confirm the presence of a high concentration of C in the wear region (Fig. 3a1), indicating the formation of a transfer layer composed of the PG nanoflakes. In addition, the transfer layer in the wear region has a high concentration of O (Fig. 3a2), which can be ascribed to partial oxidation of PG. To further confirm the chemical composition, Raman spectra were obtained from different regions of the wear scar (inset of Fig. 3a;

the regions for the Raman spectra are marked with the same color as the corresponding Raman spectrum profile). The D and G peaks in the Raman spectra indicate the presence of graphene nanoflakes in the wear scars. However, in contrast to the original PG nanoflakes (Fig. S1i), the Raman spectra obtained from the wear region of the steel ball had a higher I_D/I_G ratio, which can be ascribed to defects and partial oxidation of the PG nanoflakes. The wear track on the steel substrate had a smooth surface without visible grooves after the friction test at 2 N (Fig. 3b), which is consistent with the 3D morphology results. The top layer of the PG nanoflake cluster were exfoliated; however, a randomly distributed tribofilm containing PG nanoflakes was still observed in the wear track center area, which was also observed at the edge of the wear track (Figs. 3b and S15), as verified by both the EDS mapping (Figs. 3b1–3b3) and Raman spectra (inset of Fig. 3b). In the regions without an obvious tribofilm, the characteristic Raman peaks of the graphene structure can also be detected, although a low concentration of graphene nanoflakes led to a relatively weak intensity. The results suggest that the PG coating can effectively protect the friction pairs during friction tests at 2 N. In contrast, when the friction tests were conducted at 100 N, wear of the steel ball can be clearly observed (Fig. 3c). Although the presence of C in the transferred PG nanoflakes was also detected in the wear scar area, a dense transfer layer was not uniformly formed on the surface of the steel ball (Figs. 3c1–3c3; inset of Fig. 3c), leading to severe wear of the steel ball. A significant wear with a maximum depth of a wear track of approximately 2 μm (Fig. S9g) was also observed on the steel substrate with the PG coating at 100 N (Fig. 3d). Clear grooves were detected in the contact region of the steel

substrate (Fig. S16), which can be attributed to the failure to form a dense tribofilm containing PG nanoflakes in the wear track at a normal load of 100 N (Figs. 3d1–3d3), leading to a relatively poor wear resistance behavior.

After the friction tests, the chemical composition of the wear track region was further examined using X-ray photoelectron spectroscopy (XPS) to reveal the possible tribochemical behavior (Figs. 3e–3i). The original PG nanoflakes exhibited limited oxidation before the tests. However, the rubbing process resulted in a significant oxidation of the PG nanoflakes (Fig. 3h), with higher oxidation observed at 100 N compared to 2 N. The C 1s spectra showed that the original PG nanoflakes had a high concentration of sp^2 -bonded carbon. The peak for sp^3 -bonded carbon and a small peak for C–O bonds were also observed in the C 1s spectra (Fig. 3e). In the friction test at 2 N, the concentration of sp^2 -bonded carbon decreased (Figs. 3f and 3i), indicating damage to the graphene structure. Meanwhile, the appearance of the peak for C=O bonds was accompanied by oxidation of the graphene nanoflakes by rubbing. The concentrations of C–O and C=O bonds after the friction test at 100 N were higher compared with those after the test at 2 N, indicating that the rubbing process at higher contact pressure resulted in more severe oxidation of PG.

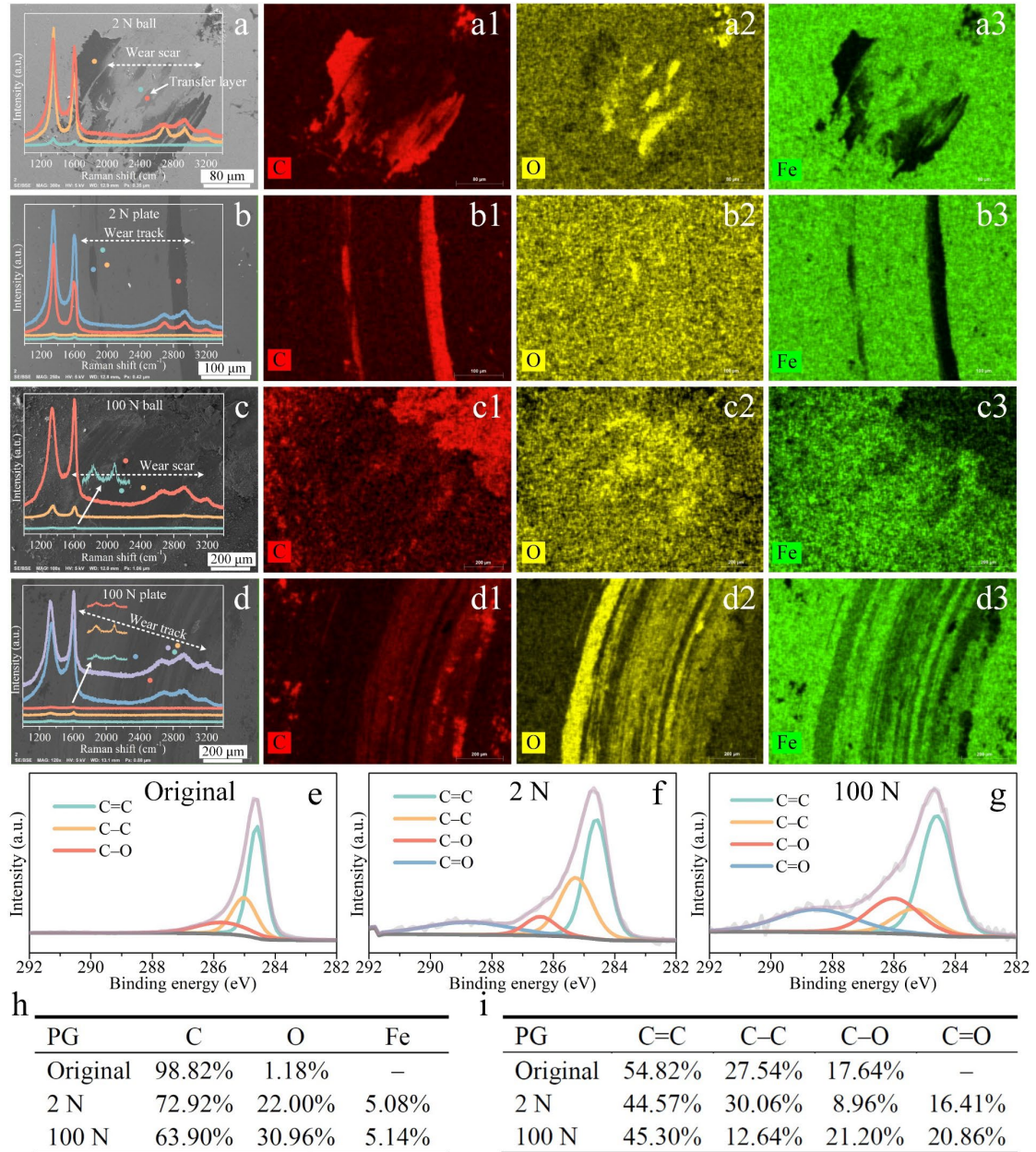


Figure 3. Characterization of the wear regions with PG coatings as solid lubricants (2 N/100 N, 1200 s). (a) SEM image and Raman spectra of the wear scar on the steel ball (2 N); EDS mapping of (a1) C, (a2) O, and (a3) Fe. (b) SEM image and Raman spectra of the wear track (2 N) on the steel substrate; EDS mapping of (b1) C, (b2) O, and (b3) Fe. (c) SEM image and Raman spectra of the wear region on the steel ball (100 N); EDS mapping of (c1) C, (c2) O, and (c3) Fe. (d) SEM image and Raman spectra of the wear track (100 N) on the steel substrate; EDS mapping of (d1) C, (d2) O, and (d3) Fe. C 1s XPS spectrum for (e) original PG nanoflakes, and the wear tracks at normal loads of (f) 2 N and (g) 100 N. (h, i) Comparison of the chemical composition of the wear regions.

2.2.2 Graphene oxide coating

The wear regions in GO coatings exhibited a distinct morphology compared to those in PG coatings. After the friction tests of the GO coating at normal loads of 2 N (Figs. 4a, 4a1–4a3) and 100 N (Figs. 4c, 4c1–4c3), a high concentration of C was detected on the surface of the steel balls, suggesting that the transfer layers with GO nanoflakes can be successfully formed during friction tests at both low and high normal loads, which was also verified using the Raman spectra (insets of Figs. 4a and 4c). For the steel substrates deposited with GO coating, the wear track regions at normal loads of 2 N (Figs. 4b and 4b1–4b3) and 100 N (Figs. 4d and 4d1–4d3) were mainly covered with densely stacked GO nanoflakes, which effectively reduced the wear. The Raman spectra (insets of Figs. 4b and 4d) indicate that the I_D/I_G ratio in the wear regions was slightly higher than that of the original GO nanoflakes before the tests. This increase can be attributed to the defects caused by the friction process.

XPS was used to evaluate the chemical composition of the wear region (Figs. 4e–4i). The full spectral results show that the friction process resulted in a significant reduction in GO (Figs. 4h), where the concentrations of O were similar in the wear tracks at 2 N and 100 N. The C 1s spectra showed that the original GO nanoflakes had a high concentration of sp^2 -bonded carbon, high concentration of C–O bonds, and relatively low content of C=O bonds (Figs. 4e and 4i). After the friction test at 2 N, peaks for sp^3 -bonded carbon and O–C=O appeared, whereas the concentration of C–O/C=O bonds decreased, corresponding to the reduction of GO (Figs. 4f and 4i). In contrast, the

concentration of C–O bonds significantly decreased after the friction test at 100 N, and a new peak centered at 282.2 eV appeared (Figs. 4g and 4i), which can be ascribed to the formation of C–Fe bonds [46].

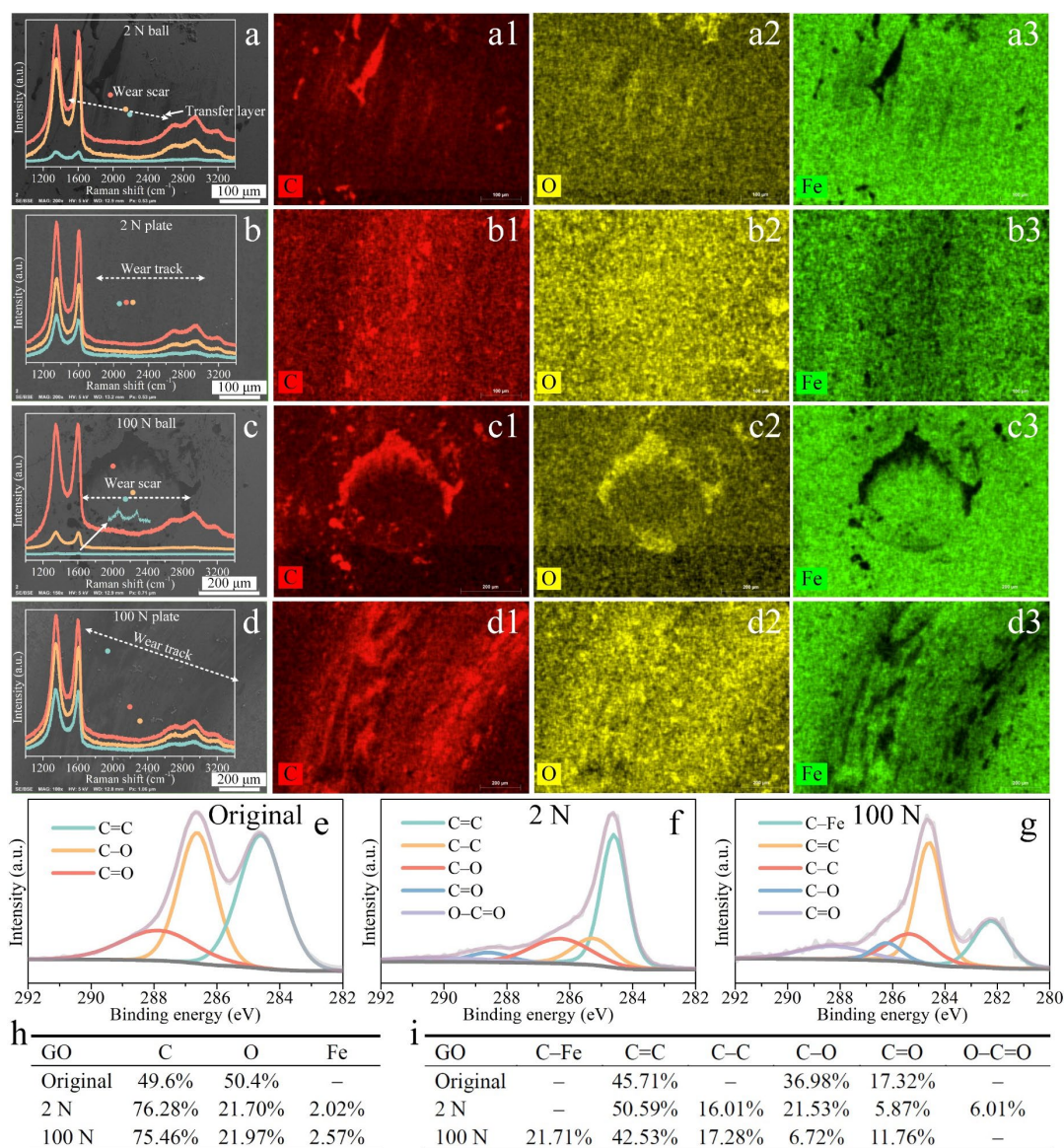


Figure 4. Characterization of the wear regions with GO coatings as solid lubricants (2 N/100 N, 1200 s). (a) SEM image and Raman spectra of the wear scar on the steel ball (2 N); EDS mapping of (a1) C, (a2) O, and (a3) Fe. (b) SEM image and Raman spectra of the wear track (2 N) on the steel substrate; EDS mapping of (b1) C, (b2) O, and (b3) Fe. (c) SEM image and Raman spectra of the wear scar on the steel ball (100 N); EDS mapping of (c1) C, (c2) O, and (c3) Fe. (d) SEM image and Raman spectra of the wear track (100 N) on the steel substrate; EDS mapping of (d1) C, (d2) O, and (d3) Fe. C 1s XPS spectrum for (e) original GO coating, and the wear tracks at normal loads of (f) 2 N and (g) 100 N. (h, i) Comparison of the chemical composition of the wear regions.

2.2.3 Fluorinated graphene coating

When lubricated with FG coating at 2 N, a transfer layer containing FG nanoflakes was identified in the wear scar region on the surface of the steel ball (Figs. 5a and 5a1–5a4). Although the top layer of FG nanoflake cluster was exfoliated, the tribofilm containing FG nanoflakes was formed on the surface of the wear track on the steel substrate at 2 N (Figs. 5b and 5b1–5b4; Fig. S17). After the friction test at 100 N, the EDS mapping results for the wear scar of the steel ball (Figs. 5c1–5c4) and wear track of the steel substrate (Figs. 5d1–5d4) showed that the wear regions had a lower concentration of F than the wear regions after the friction test at 2 N. In addition, the concentration of O increased substantially in the wear regions at 100 N compared with that in the FG coating before the test, suggesting that the rubbing process at a high normal load was accompanied by severe oxidation. Quantitative EDS results were also obtained from the wear scar to better elucidate the chemical composition of the wear region where the C and F contents can be detected (Fig. S18). The high-resolution SEM-EDS images of the wear track at 100 N showed that the regions with high concentrations of C were randomly distributed in the wear track (Figs. S19 and S20). It can be concluded from a combination of the EDS and Raman spectra results (insets of Figs. 5c and 5d) that the formation of the transfer layer and tribofilm for the FG nanoflakes on the surfaces of the friction pairs can be realized at both a low normal load of 2 N and high normal load of 100 N, providing excellent lubrication and wear resistance performance.

The chemical compositions of the wear track regions under lubrication by FG coatings

at 2 N and 100 N exhibited significant differences (Figs. 5e–5l). The full spectra results showed that the F content of FG nanoflakes decreased from 50.26% to 31.83% and 4.61% after the friction process at normal loads of 2 N and 100 N, respectively, whereas the O content increased from 0.66% for the original FG nanoflakes to 7.40% and 24.07% after the friction process at normal loads of 2 N and 100 N, respectively (Figs. 5k and 5l). Elevated normal loads led to a more pronounced reduction and oxidation of FG nanoflakes compared to that observed at lower normal loads. The C 1s spectrum showed that the original FG nanoflakes have high concentrations of C–F and C–F₂ bonds. Furthermore, a relatively low content of sp²-bonded carbon was observed (Figs. 5e). In the F 1s spectrum, a peak for F–C bonds was also simultaneously observed (Fig. 5h). After the friction test at 2 N, a peak was observed for sp³-bonded carbon, and the area ratio of the peak for the C–O bonds increased from 9.07% in the original FG nanoflakes to 25.10%. Meanwhile, the decrease in the concentration of C–F₂ bonds indicates the breakage of C–F bonds in the basal plane.

In contrast, after the friction test at 100 N, a peak was observed for sp³-bonded carbon, and a significant decrease in the concentration of C–F and C–F₂ bonds was observed. Additionally, in the F 1s spectrum, a new peak for ionic F–Fe bonds occurred (Fig. 5j), which can be ascribed to the breakage of F–C bonds and the tribochemical reaction as a result of the rubbing process at high contact pressures. It should be noted that the formation of F–Fe bonds contributes to the formation of FG-containing tribolayers on their counterparts, leading to the enhanced tribological behavior of the FG coating.[46,

47] Based on the results, it can be concluded that the exceptional solid lubrication performance of the FG coating under ultrahigh contact pressure is closely associated with the formation of distinctive island-like tribolayers through tribochemical reactions. Additionally, the inherent low interlaminar shear strength between the lattice layers of FG contributes to this performance. In comparison, the chemical inertness of PG hindered the formation of robust tribolayers under ultrahigh contact pressures. On the other hand, GO's high interlayer shear strength induced by the O-containing groups resulted in relatively poor solid lubrication behaviors when compared to FG.

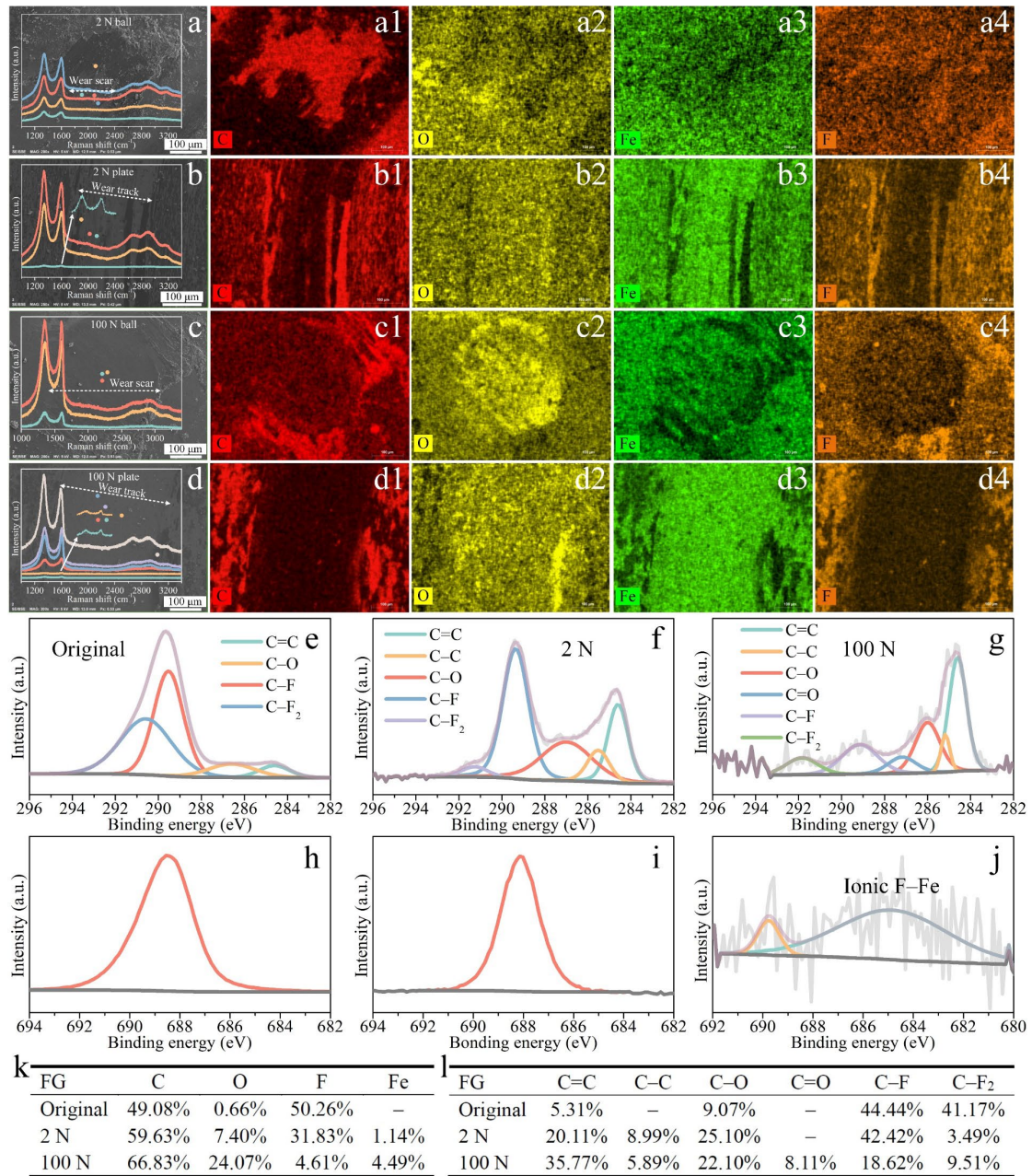


Figure 5. Characterization of the wear regions with FG coatings as solid lubricants (2 N/100 N, 1200 s). (a) SEM image and Raman spectra of the wear scar on the steel ball (2 N); EDS mapping of (a1) C, (a2) O, (a3) Fe, and (a4) F. (b) SEM image and Raman spectra of the wear track (2 N) on the steel substrate; EDS mapping of (b1) C, (b2) O, (b3) Fe, and (b4) F. (c) SEM image and Raman spectra of the wear scar on the steel ball (100 N); EDS mapping of (c1) C, (c2) O, (c3) Fe, and (c4) F. (d) SEM image and Raman spectra of the wear track (100 N) on the steel substrate; EDS mapping of (d1) C, (d2) O, (d3) Fe, and (d4) F. High resolution (e–g) C 1s and (h–j) F 1s XPS spectra results for original GO coating, and the wear tracks at normal loads of 2 N and 100 N. (k, l) Comparison of the chemical composition of the wear regions.

2.2.4 MoS₂ coating

MoS₂ coatings were also investigated in addition to the graphene coatings discussed in the previous section. As demonstrated in section 2.1.2, a robust superlubricity can be achieved for MoS₂ coating under a normal load of 400 N. Therefore, the counterparts after the friction tests under normal loads of 2 N and 400 N were compared to unveil the interfacial structural changes induced by contact pressure and elucidate the superlubricity mechanism under ultrahigh contact pressure. When lubricated with MoS₂ coating at 2 N, tribolayers were formed on the surface of the counterparts, a fact supported by both the SEM images (Figs. 6a and 6b) and the EDS mapping results (Figs 6a1–6a4 and 6b1–6b4). However, these tribolayers were not uniform and have varied thickness as can be observed in Figure. 6a1 and 6b1. In contrast, under a high normal load of 400 N, the tribolayers have more homogeneous structure (Fig. 6c, 6c1–6c4, 6d and 6d1–6d4).

The chemical compositions of friction pairs after the tests under 2 N and 400 N, were further investigated (Figs. 6e–6j). The Mo 3d spectra were deconvoluted to differentiate the Mo⁴⁺ and Mo⁶⁺, where the increased area ratio of the peak for Mo⁶⁺ [48, 49] can be attributed to the formation of MoO₃ by rubbing. It is interesting to note, that for both counterpart surfaces after the friction tests under a high normal load of 400 N, the area ratios of the peaks for Mo⁶⁺ were all lower than that under a low normal load of 2 N (Fig. 6j), indicating that the oxidation of MoS₂ nanoflakes can be suppressed by the ultrahigh contact pressure, which can further explain the robust macroscale structural

superlubricity over 15,000 s under a high normal load of 400 N (Fig. 2e).

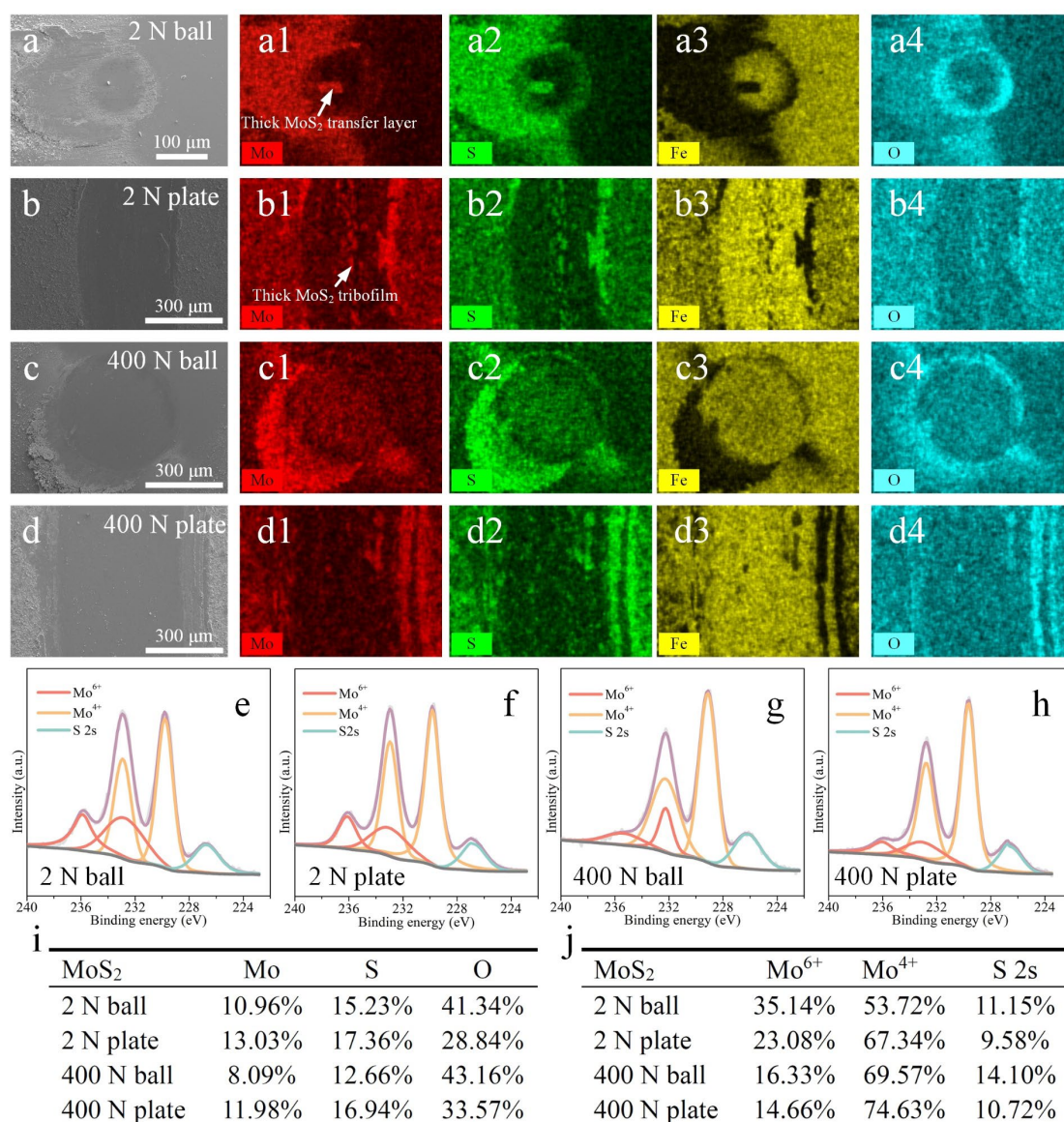


Figure 6. Characterization of the wear regions with MoS₂ coatings as solid lubricant (2 N/400 N, 1200 s). (a) SEM image of the wear scar on the steel ball (2 N); EDS mapping of (a1) Mo, (a2) S, (a3) Fe, and (a4) O. (b) SEM image of the wear track (2 N) on the steel substrate; EDS mapping of (b1) Mo, (b2) S, (b3) Fe, and (b4) O. (c) SEM image of the wear scar on the steel ball (400 N); EDS mapping of (c1) Mo, (c2) S, (c3) Fe, and (c4) O. (d) SEM image of the wear track (400 N) on the steel substrate; EDS mapping of (d1) Mo, (d2) S, (d3) Fe, and (d4) O. High resolution (e–h) Mo 3d XPS spectra results for the wear scars and wear tracks at a normal of (e, f) 2 N and (g, h) 400 N. (i, j) Comparison of the chemical composition of the wear regions, where the elemental compositions in (i) are for the comparison between the ratios of Mo, S and O.

2.3 Pressure-induced tribolayer structural evolution

In addition to the formation of tribolayers, the nanostructure of these tribolayers plays a critical role in influencing the macroscale solid lubrication behaviors. Among the graphene coatings, FG coating exhibited the best lubrication performance under high normal loads. To elucidate the underlying mechanisms of the stress dependent lubrication behaviors of FG coating, the nanostructures of tribolayers were examined by High-resolution transmission electron microscope (HRTEM) of the cross-sectional lamellar samples extracted by focused ion beam (FIB) from the wear regions. After the friction test at 2 N, a tribofilm can be observed between the steel substrate and the deposited Cr protecting layer in the wear track (Figs. 7 and S21). Two different tribofilm regions were identified in the high-angle annular dark-field (HAADF) scanning transmission electron microscope (STEM) image (Fig. 7a). The EDS mapping results (Figs. 7b–7e) indicate that the black region of the tribofilm had a high concentration of C, corresponding to FG nanoflakes, whereas the light gray region of the tribofilm had high concentrations of Fe and O, corresponding to Fe oxides. The HRTEM images show that the tribofilm had a thickness of approximately 20–40 nm, and the FG nanoflakes and Fe oxide layers were alternately distributed within the tribofilm (Figs. 7f and 7g). The TEM-EDS results suggest that the typical layered structure of FG was maintained during the tests at a normal load of 2 N. In addition, the Fe oxide layers within the tribofilm can be attributed to the structural transformation of wear particles.

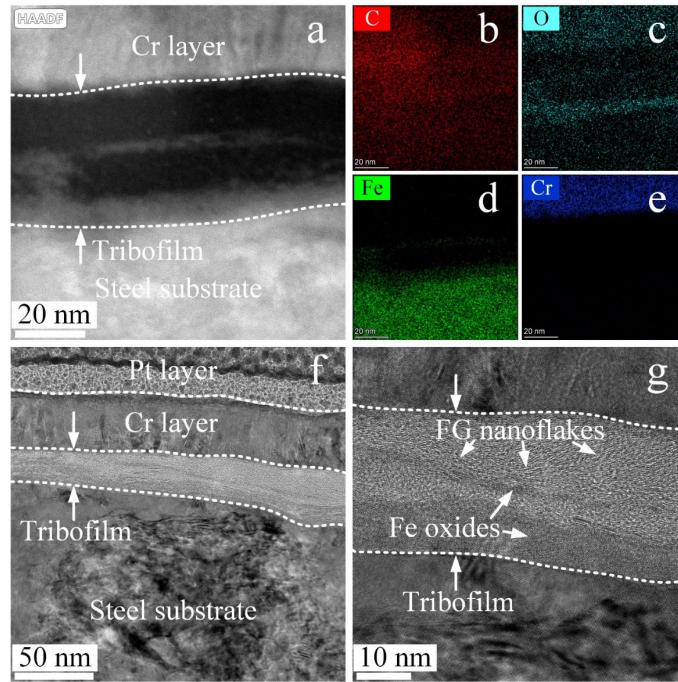


Figure 7. Cross-sectional analysis of the wear track on the steel substrate with FG coating (2 N, 1200 s). (a) HAADF-STEM image and EDS mapping of (b) C, (c) O, (d) Fe, and (e) Cr. (f) Tribofilm containing FG nanoflakes formed during the friction process, where the (g) layered structure of FG nanoflakes can be examined.

In contrast the tribofilm formed at a low normal load of 2 N, characterized by an alternating nanostructure with FG nanoflakes and Fe oxides, the tribolayers formed at a high normal load of 100 N exhibit a completely different nanostructure. The HAADF-STEM image (Fig. 8d) and EDS mapping results (Figs. 8e–8h) of the wear scar on the steel ball, revealed that the distributions of C (corresponding to FG nanoflakes), Fe, and O (corresponding to Fe oxides) were uniform in the transfer layer formed at a high normal load of 100 N, which can also be verified from the HRTEM image (Fig. 8i). Similar results were obtained for the cross-sectional samples of the wear track on the steel substrate (Figs. 8j–8o and S22). These results confirmed the formation of nanocomposite tribolayers with uniformly distributed FG nanoflakes and Fe oxides under high contact pressure.

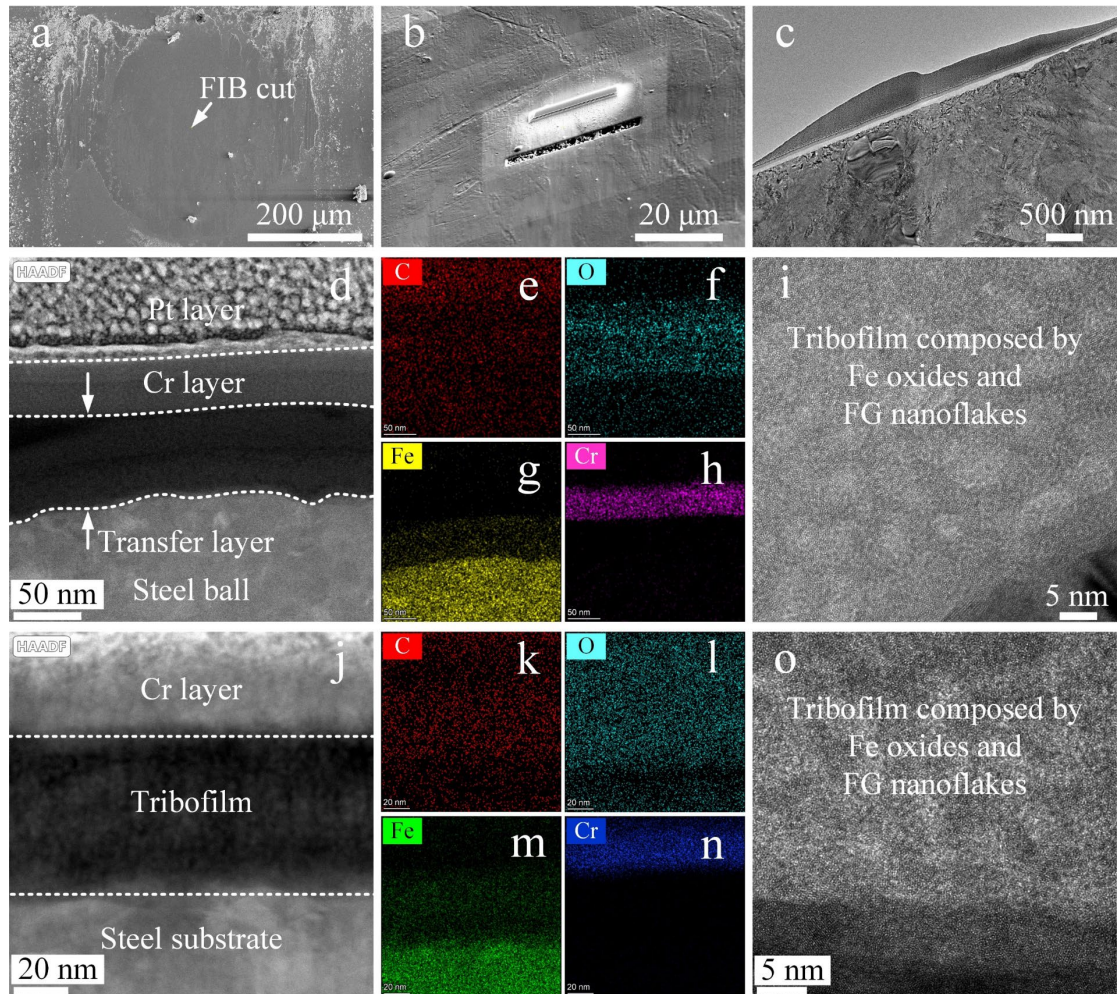


Figure 8. Cross-sectional analysis of the wear scar on the steel ball and the wear track on the steel substrate with FG coating (100 N, 1200 s). (a, b) Location of the lamellar sample extracted from the wear scar, and the (c) corresponding TEM image. (d) HAADF-STEM image, and EDS mapping of (e) C, (f) O, (g) Fe, and (h) Cr. (i) HRTEM image of the transfer layer. (j) HAADF-STEM image of the tribofilm on the steel substrate, and EDS mapping of (k) C, (l) O, (m) Fe, and (n) Cr. (o) HRTEM image acquired from the tribofilm region.

While FG coating can offer stable lubrication with a low COF of 0.041 under a normal load of 400 N, there is still a gap to reach the superlubricity state with a COF lower than 0.01. In contrast, robust superlubricity can be achieved with the MoS₂ coating. To unravel the underlying mechanisms for the distinct macroscale tribological behavior under high contact pressure, the nanostructures of the tribofilms lubricated with MoS₂ coatings under 2 N and 400 N were further characterized. After the friction test at 2 N,

a tribofilm can be observed in the wear track on the steel substrate (Figs. 9 and S23). The HAADF-STEM image (Fig. 9b) and the corresponding EDS mapping results (Figs. 9c–9h) suggest that the tribofilm is composed of alternately distributed MoS₂ nanoflakes (in upper and lower regions) and Fe oxide particles (in middle region of the tribofilm). The typical layered crystal structure of MoS₂ can be clearly observed from the HRTEM image (Fig. 9i–9k). Under a low normal load of 2 N, the nanostructure of the tribofilms formed on MoS₂ coating was similar to that of FG coating. However, with high normal loads, the nanostructure of the tribofilm on MoS₂ coating exhibited significant difference from that of FG coating. Under a normal load of 400 N, the tribofilm with a MoS₂ / Fe oxides / MoS₂ sandwiched nanostructure can be observed (Figs. 10a–10g; Fig. S24). Moreover, under that high normal load, extremely thin tribofilm with a few highly oriented MoS₂ layers can be observed (Figs. 10h and 10i). Most importantly, it should be noted that the layered structure of MoS₂ is highly aligned with the sliding direction and can be retained even under a high contact pressure of 3.55 GPa.

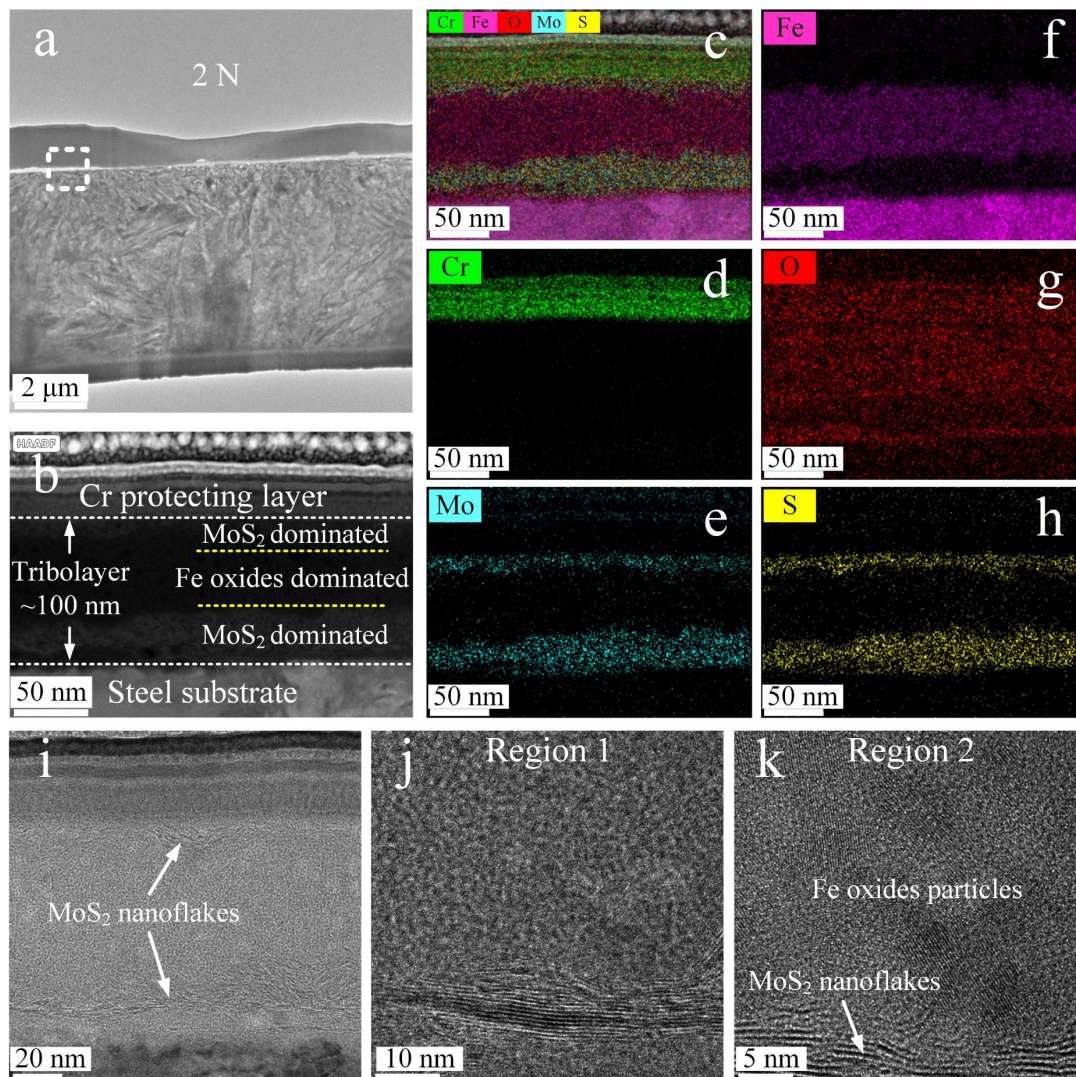


Figure 9. Cross-sectional analysis of the wear track on the steel substrate with MoS₂ coating (2 N, 1200 s). (a) TEM image of the lamellar sample extracted from the wear track, where the tribofilm region for HRTEM-EDS characterization is marked. (b) HAADF-STEM image, and EDS mapping of (c) mixed elements, (d) Cr, (e) Mo, (f) Fe, (g) O and (h) S. (i–k) HRTEM images of the tribofilm.

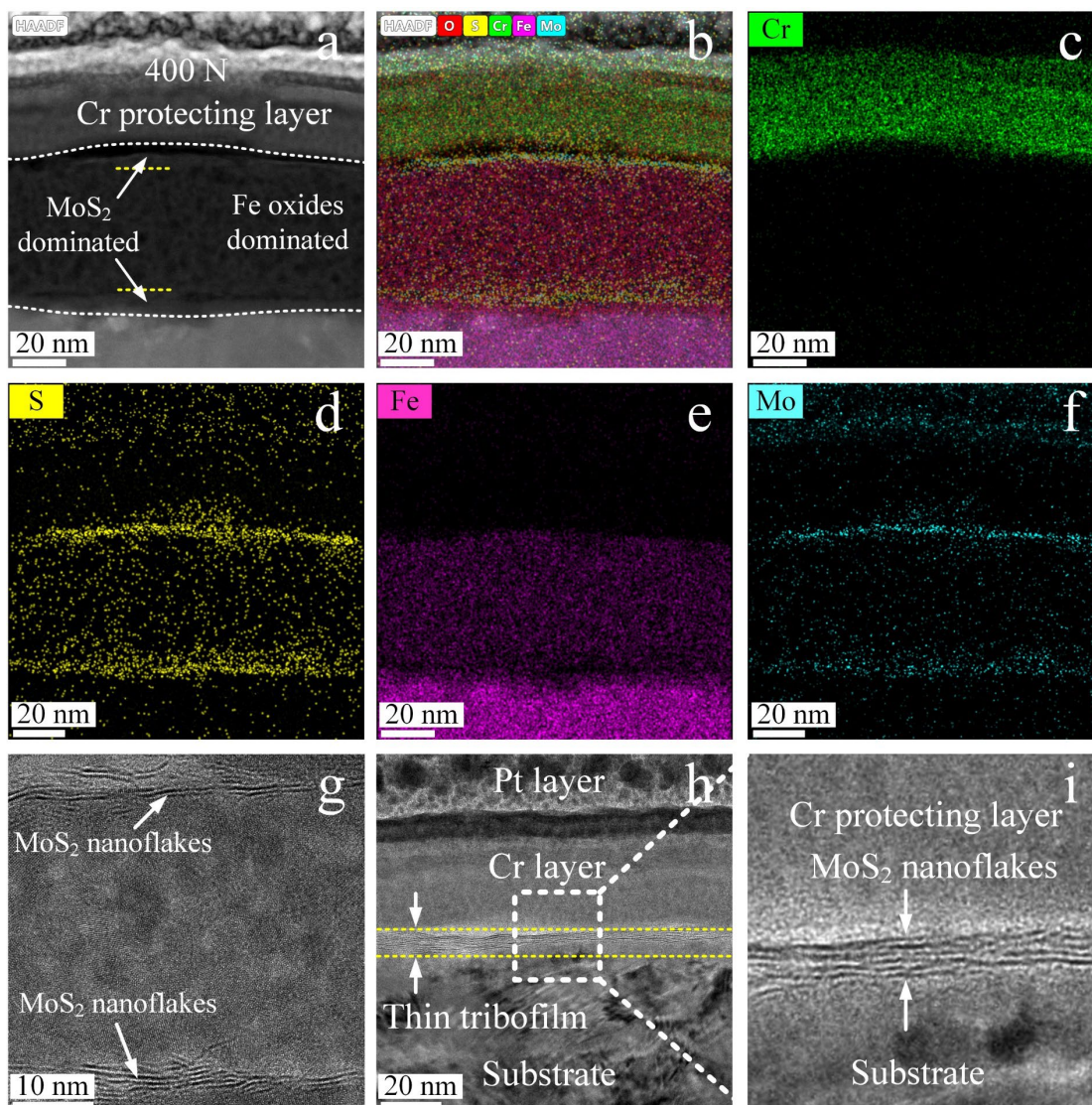


Figure 10. Cross-sectional analysis of the wear track on the steel substrate with MoS₂ coating (400 N, 1200 s). (a) HAADF-STEM image, and EDS mapping of (b) mixed elements, (c) Cr, (d) S, (e) Fe, and (f) Mo. (g, h) HRTEM images of two different regions of the tribofilm. (i) Enlarged HRTEM image of the region marked in (h).

3 Discussion

The above results demonstrate that the ultralow friction of 2D materials as solid lubricants is highly correlated with the formation of robust tribolayers tribochemical reactions and the interfacial structural evolution. Generally, the tribolayers formed in-situ during the rubbing process are critical for the tribological performance of those materials.[50-52] For the graphene-based coatings used in this study (PG, GO, and FG),

tribolayers can be formed at a low normal load, which can provide effective lubrication and wear resistance. However, as the normal load increased to 100 N, the formation of dense tribolayers with PG nanoflakes on the surface of the wear regions became challenging, leading to severe wear of the counterparts. In contrast, with GO coating acting as a solid lubricant, a dense tribofilm was formed over the entire wear track at a normal load of 100 N, resulting in the least wear among the three graphene-based coatings. With FG coating as a solid lubricant, island-like tribolayers with a relatively small thickness were formed, which yielded the lowest COF among the graphene-based coatings. The wear of the friction pairs was also significantly suppressed by FG coating.

The formation process of tribolayers and their effect on the lubrication and wear resistance are important in solid lubrication phenomenon. In a macroscale tribological system, the contact region can be regarded as a collection of several discrete microcontact regions. The mechanism of tribolayer formation on contact asperities under graphene lubrication has been investigated using atomic force microscope (AFM) [53]. The study revealed that the formation of a tribolayer is a competition between the interlayer force of the graphene layers and the interface force between graphene and the surface of the contact asperities. A high interfacial force between the contact asperities and the top-layer graphene can promote the exfoliation of graphene, and hence, the tribolayer formation. [53]

In our study, the bonding and shear strengths between the surface of the steel

counterparts and PG nanoflakes during the friction process at high normal loads were lower than those of the GO nanoflakes (which can be attributed to the high surface energy of GO) and FG nanoflakes (owing to the formation of ionic Fe–F bonds) [54]. Therefore, at high normal loads, it is difficult for robust tribolayers to be formed when PG coating is used as a solid lubricant, leading to severe wear and additional energy dissipation. In contrast, for GO coating, dense tribolayers are formed, which can be ascribed to the strong adhesion between the counterpart surface and GO [55] and between the GO layers itself, leading to suppressed wear and stable lubrication performance. In contrast to the GO nanoflakes, the original FG nanoflakes exhibited low adhesion to the steel counterparts. However, the ionic F–Fe bonds formed under high normal loads promoted the formation of tribolayers on the contact asperities. Meanwhile, the adhesion strength and shear strength between the lattice layers of the FG nanoflakes were lower than those of the PG and GO nanoflakes [56, 57], making it difficult to form large-area tribolayers on their counterparts, similar to that of lubrication by GO coating. This explains the formation of island-like tribolayers on the contact asperities for FG coatings (Fig. 5). The tribolayers formed in situ transfer the sliding between the counterparts to that between FG nanoflakes, where the interlayer shear strength of FG is lower than those of PG and GO [57]. This dominance in interlayer shear strength plays a crucial role in determining the macroscale lubrication performance of the FG coating.

It is widely accepted that, for 2D materials as macroscale solid lubricants, the interlayer

slippage between lattice layers predominantly governs the lubrication behavior. Although GO and FG coatings can effectively provide lubrication even under a high normal load of 400 N, achieving a low COF of 0.041 with FG coating, the COF with the lubrication of graphene family coatings remains higher than that of MoS₂ coating by more than an order of magnitude. Interestingly, both the molecular dynamic simulation [58] and the density functional theory calculation [59] suggest that the interlayer shear strength between PG lattice layers is lower than that of MoS₂ [60, 61]. The interlayer shear strength of PG can be further reduced by fluorination [57]. The mismatch between the interlayer shear strength and the macroscale frictional performance can be attributed to the dynamic interfacial structural evolution induced by rubbing. For FG coating, the typical layered structure can be clearly observed from the cross-sectional HRTEM images after the rubbing process under a low normal load of 2 N (Fig. 7). However, the structure of FG nanoflakes deteriorated under a relatively high normal load of 100 N (Fig. 8). Tribolayers composed of Fe oxide particles and deteriorated FG nanoflakes were formed on the counterparts rather than layered structures aligned with the sliding direction. In contrast, the layered lattice structure was retained for MoS₂ coating under both a low normal load of 2 N (Fig. 9) and a high normal load of 400 N (Fig. 10), which led to lower macroscale COF comparing with the FG coating.

MoS₂ coating can provide superlubricity under ambient conditions with normal loads higher than 100 N. Hertzian contact theory was used to explain the reduced COF under

higher normal loads [62, 63]. Recently, the densification of the tribolayers formed in situ and reorientation of the lattice layers have been considered as the predominant mechanism for the reduced COF at high contact pressures.[52] With this mechanism, it can be assumed that if the dense tribolayers with highly oriented layered phases formed under high contact pressures contribute to the reduced COF at high contact pressures, these tribolayers can still provide a lower COF when the applied normal load suddenly decreases to a lower value. Hence in this work, additional friction tests with normal loads varied during a single experiment were conducted to test the hypothesis (Fig. S25). We observed, that the COF recovered from the superlubricity state to higher value, reaching 0.05–0.06 when the normal load decreased from 400 N to 10 N.

It can be deduced that the shear strength at the sliding interface decreased through a simple Hertzian contact theory calculation. The trend of decreased shear strength with increased contact pressure becomes more pronounced when accounting for the real contact area between rough surfaces [64]. However, it is likely that the observed macroscale structural superlubricity of MoS₂ coating was not only due to the specific contact mechanics conditions [65, 66] and resulting densification of the tribolayers and lattice layers reorientation. Recent studies indicate that the real time response of tribolayer nanostructures to the external stress also have potential impact on the solid lubrication behaviors. Deng et al. [67] evaluated the nanoscale tribological performance of chemically-modified graphite using AFM. An unusually negative coefficient of friction was observed due to high adhesion between the AFM tip and the sample surface.

This phenomenon depends on the ratio of adhesion between the AFM tip and samples to the exfoliation energy of the chemically-modified graphite. This phenomenon was attributed to the reversible partial delamination of the topmost single- or a few-layer thick graphene clusters, where increased normal load at the asperities resulted in suppressed deformability, and hence, a smaller energy loss induced by the displacement of the deformed region.

Furthermore, elevated normal pressure can induce distinctive behaviors in 2D materials. At the atomic scale, the dissipation of frictional energy is intricately connected to the sliding potential energy between the lattice layers of 2D materials. Through dispersion-corrected density functional calculations, it has been revealed that the sliding potential energy can transition from being corrugated to substantially flattened with increased contact pressure [68]. These mechanisms may also contribute to the macroscale structural superlubricity observed in MoS₂ coating under ultrahigh contact pressure.

In addition to the nanostructure of tribolayers, the impact of environmental humidity is in particular critical for the lubrication behavior of MoS₂. Previous studies reported that superlubricity of MoS₂ based coatings is usually limited to vacuum conditions [69-71]. Under ambient condition, the dissociation of water molecules results in the formation of Mo–O–Mo chemical bonds, whereas undissociated water molecules adsorbed between lattice layers of MoS₂ contribute to increased friction, leading to the failure of superlubricity. [45] Our results demonstrate however, that macroscale structural

superlubricity can be also achieved under ultrahigh contact pressures in ambient conditions (Fig. 2). The diminished adsorption of water molecules under ultrahigh contact pressure can be one of the mechanisms for the achievement of macroscale structural superlubricity. On the one hand, diminished water molecules adsorption can suppress the formation of defects and oxidation of MoS₂ nanoflakes by dissociated water molecules (Figs. 6e–6j). On the other hand, the diminished water molecules adsorption can also eliminate the frictional energy dissipation by physically adsorbed undiminished water molecules between lattice layers. Hence, for the first time, we present evidence that the inhibited influence of water molecules under ultrahigh contact pressure is critical for achieving robust, long-duration structural superlubricity under ambient conditions (Fig. 2e). Our findings reveal the underlying mechanisms for the macroscale structural superlubricity under ultrahigh contact pressure, where the formation of robust tribolayers, maintaining the easy-shearing plane between the lattice layers of 2D materials, and the eliminated influence of external environment are all critical. Meanwhile, the dynamic evolution of the interfacial structure governing distinct macroscale lubrication behaviors of 2D materials as solid lubricants under varied contact pressures was also elucidated. Our findings offer fundamental insights into the lubrication mechanisms of 2D materials as solid lubricants under diverse contact pressures, with implications for advancing their engineering applications in harsh and complicated working conditions.

4 Conclusions

Our work showcases the achievement of robust macroscale structural superlubricity, characterized by a COF of approximately 0.004, between steel counterparts lubricated with 2D materials under ambient conditions and an ultrahigh contact pressure of around 3.55 GPa. This represents a highly desirable macroscale lubrication behavior, significantly expanding the potential of 2D materials as solid lubricants for engineering applications. A thorough analysis reveals the dynamic interfacial structural evolution under varied contact pressures, which is the primary factor influencing the diverse macroscale lubrication behaviors of 2D materials. Furthermore, ultrahigh contact pressure induces changes in adsorption and tribochemical behaviors, playing a critical role in realizing macroscale structural superlubricity under ambient conditions. These findings carry substantial significance for the future design and application of 2D materials as solid lubricants in harsh and complicated working conditions.

Experimental procedures

Brief experiment setups are presented here, while very detailed procedures please find in the first section of the **Supporting Information**.

Materials

AISI52100 steel plates and steel balls were used as counterparts. PG (product number of XF182-1), GO (product number of XF002-1), and FG (product number of XF225) nanoflakes powders were provided by XFNANO Materials Technology (China). TMDs nanoflakes including MoS₂ (product number of M104968) and WS₂ (product number

of T137743) nanoflakes were provided by Aladdin Scientific Corp., Shanghai, China.

Preparation of solid lubrication coatings and friction tests

Solid lubrication coatings of 2D materials were drip casted onto steel substrates. Macroscale friction tests were conducted under a velocity of 12.56 mm/s, and normal loads from 2–400 N (corresponding to Hertz contact pressures of 0.61–3.55 GPa) with a universal microtribotester (UMT-3, Bruker, USA; ball-on plate mode). Each friction test was repeated at least three times to obtain more reliable results.

Surface Characterization

The surface morphologies and wear rates of the counterparts after friction tests were obtained using a 3D white light interferometer to investigate the anti-wear performances of solid lubrication coatings. The topography and chemical composition of the contact regions were observed using a FESEM-EDS. The chemical structures and the concentration of different chemical groups were further characterized by Raman and XPS. The lamellar samples of the contact regions were prepared by a FIB–SEM dual system, then characterized by HRTEM-EDS to further reveal the dynamic evolution of tribolayers nanostructures.

Acknowledgements

This work was financially supported by the National Key Research and Development Program of China (grant number 2021YFB3400200), National Natural Science Foundation of China (grant number 52005287), Hebei Natural Science Foundation (grant number E2024105063), Beijing Institute of Technology Research Fund Program for Young Scholars, Tribology Science Fund of State Key Laboratory of Tribology in Advanced Equipment (SKLT) (grant number SKLTKF21B14), and Young Elite Scientists Sponsorship Program by BAST (grant number BYESS2023288). The authors acknowledge the Analysis & Testing Center, Beijing Institute of Technology for the use of the FIB and HRTEM.

References

- [1] J. Luo, X. Zhou, Superlubricative engineering—Future industry nearly getting rid of wear and frictional energy consumption, *Friction* 8(4) (2020) 643-665.
- [2] J.M. Martin, H. Pascal, C. Donnet, T. Le Mogne, J.L. Loubet, T. Epicier, Superlubricity of MoS₂: crystal orientation mechanisms, *Surface and Coatings Technology* 68-69 (1994) 427-432.
- [3] C. Donnet, J.M. Martin, T. Le Mogne, M. Belin, Super-low friction of MoS₂ coatings in various environments, *Tribology International* 29(2) (1996) 123-128.
- [4] A. Erdemir, O.L. Eryilmaz, G. Fenske, Synthesis of diamondlike carbon films with superlow friction and wear properties, *Journal of Vacuum Science & Technology A* 18(4) (2000) 1987-1992.
- [5] X. Chen, C. Zhang, T. Kato, X.-a. Yang, S. Wu, R. Wang, M. Nosaka, J. Luo, Evolution of tribo-induced interfacial nanostructures governing superlubricity in a-C:H and a-C:H:Si films, *Nature Communications* 8(1) (2017) 1675.
- [6] Q. Jia, Z. Yang, L. Sun, K. Gao, B. Zhang, X. Zhang, J. Zhang, Catalytic superlubricity via in-situ formation of graphene during sliding friction on Au@a-C:H films, *Carbon* 186 (2022) 180-192.
- [7] D. Zhu, H. Li, L. Ji, H. Zhou, J. Chen, Tribochemistry of superlubricating amorphous carbon films, *Chemical Communications* 57(89) (2021) 11776-11786.
- [8] A.A. Voevodin, J.P. O'Neill, J.S. Zabinski, Nanocomposite tribological coatings for aerospace applications, *Surface & Coatings Technology* 116 (1999) 36-45.
- [9] Y.-F. Liu, T. Liskiewicz, A. Yerokhin, A. Korenyi-Both, J. Zabinski, M. Lin, A. Matthews, A.A. Voevodin, Fretting wear behavior of duplex PEO/chameleon coating on Al alloy, *Surface and Coatings Technology* 352 (2018) 238-246.
- [10] Y. Liu, X. Chen, J. Li, J. Luo, Enhancement of friction performance enabled by synergetic effect between graphene oxide and molybdenum disulfide, *Carbon* 154 (2019) 266-276.
- [11] Y. Liu, J. Li, S. Yi, X. Ge, X. Chen, J. Luo, Enhancement of friction performance of nanocomposite fluorinated graphene and molybdenum disulfide coating by microdimple array, *Carbon* 167 (2020) 122-131.
- [12] R. Li, X. Yang, J. Zhao, C. Yue, Y. Wang, J. Li, E. Meyer, J. Zhang, Y. Shi, Operando Formation of Van der Waals Heterostructures for Achieving Macroscale Superlubricity on Engineering Rough and Worn Surfaces, *Advanced Functional Materials* 32(18) (2022) 2111365.
- [13] I. Leven, D. Krepel, O. Shemesh, O. Hod, Robust Superlubricity in Graphene/h-BN Heterojunctions, *The Journal of Physical Chemistry Letters* 4(1) (2013) 115-120.

- [14] P. Li, P. Ju, L. Ji, H. Li, X. Liu, L. Chen, H. Zhou, J. Chen, Toward Robust Macroscale Superlubricity on Engineering Steel Substrate, *Advanced Materials* 32(36) (2020) 2002039.
- [15] X. Gao, J. Zhang, P. Ju, J. Liu, L. Ji, X. Liu, T. Ma, L. Chen, H. Li, H. Zhou, J. Chen, Shear-Induced Interfacial Structural Conversion of Graphene Oxide to Graphene at Macroscale, *Advanced Functional Materials* 30(46) (2020) 2004498.
- [16] H. Liang, Y. Bu, J. Zhang, Z. Cao, A. Liang, Graphene Oxide Film as Solid Lubricant, *ACS Applied Materials & Interfaces* 5(13) (2013) 6369-6375.
- [17] X. Ge, Z. Chai, Q. Shi, Y. Liu, W. Wang, Graphene superlubricity: A review, *Friction* 11 (2023) 1953–1973.
- [18] C. Lee, Q. Li, W. Kalb, X.-Z. Liu, H. Berger, R.W. Carpick, J. Hone, Frictional Characteristics of Atomically Thin Sheets, *Science* 328(5974) (2010) 76-80.
- [19] P. Serles, M. Hamidinejad, P.G. Demingos, L. Ma, N. Barri, H. Taylor, C.V. Singh, C.B. Park, T. Filleter, Friction of $Ti_3C_2T_x$ MXenes, *Nano Letters* 22(8) (2022) 3356-3363.
- [20] B.C. Wyatt, A. Rosenkranz, B. Anasori, 2D MXenes: Tunable Mechanical and Tribological Properties, *Advanced Materials* 33(17) (2021) 2007973.
- [21] P.G. Grützmacher, S. Suarez, A. Tolosa, C. Gachot, G. Song, B. Wang, V. Presser, F. Mücklich, B. Anasori, A. Rosenkranz, Superior Wear-Resistance of $Ti_3C_2T_x$ Multilayer Coatings, *ACS Nano* 15(5) (2021) 8216-8224.
- [22] A. Rosenkranz, M.C. Righi, A.V. Sumant, B. Anasori, V.N. Mochalin, Perspectives of 2D MXene Tribology, *Advanced Materials* 35(5) (2023) 2207757.
- [23] X. Miao, Z. Li, S. Liu, J. Wang, S. Yang, MXenes in tribology: Current status and perspectives, *Advanced Powder Materials* 2(2) (2023) 100092.
- [24] S. Zhang, T. Ma, A. Erdemir, Q. Li, Tribology of two-dimensional materials: From mechanisms to modulating strategies, *Materials Today* 26 (2019) 67-86.
- [25] R. Li, C. Sun, X. Yang, Y. Wang, K. Gao, J. Zhang, J. Li, Toward high load-bearing, ambient robust and macroscale structural superlubricity through contact stress dispersion, *Chemical Engineering Journal* (2021) 133548.
- [26] M. Hirano, K. Shinjo, Atomistic locking and friction, *Physical Review B* 41(17) (1990) 11837-11851.
- [27] K. Miura, S. Kamiya, Observation of the Amontons-Coulomb law on the nanoscale: Frictional forces between MoS_2 flakes and MoS_2 surfaces, *Europhysics Letters* 58(4) (2002) 610.
- [28] J. Li, J. Li, J. Luo, Superlubricity of Graphite Sliding against Graphene Nanoflake under Ultrahigh Contact Pressure, *Advanced Science* 5(11) (2018) 1800810.
- [29] Y. Liu, A. Song, Z. Xu, R. Zong, J. Zhang, W. Yang, R. Wang, Y. Hu, J. Luo, T. Ma, Interlayer Friction and Superlubricity in Single-Crystalline Contact Enabled by Two-Dimensional Flake-Wrapped Atomic Force Microscope Tips, *ACS Nano* 12(8) (2018) 7638-7646.
- [30] D. Berman, S.A. Deshmukh, S.K.R.S. Sankaranarayanan, A. Erdemir, A.V. Sumant, Extraordinary Macroscale Wear Resistance of One Atom Thick Graphene Layer, *Advanced Functional Materials* 24(42) (2014) 6640-6646.
- [31] J. Li, T. Gao, J. Luo, Superlubricity of Graphite Induced by Multiple Transferred Graphene Nanoflakes, *Advanced Science* 5(3) (2018) 1700616.
- [32] S.-W. Liu, H.-P. Wang, Q. Xu, T.-B. Ma, G. Yu, C. Zhang, D. Geng, Z. Yu, S. Zhang, W. Wang, Y.-Z. Hu, H. Wang, J. Luo, Robust microscale superlubricity under high contact pressure enabled by graphene-coated microsphere, *Nature Communications* 8 (2017) 14029.

- [33] D. Berman, A. Erdemir, A.V. Sumant, Graphene: a new emerging lubricant, *Materials Today* 17(1) (2014) 31-42.
- [34] Y. Liu, X. Ge, J. Li, Graphene lubrication, *Applied Materials Today* 20 (2020) 100662.
- [35] L. Chen, Z. Chen, X. Tang, W. Yan, Z. Zhou, L. Qian, S.H. Kim, Friction at single-layer graphene step edges due to chemical and topographic interactions, *Carbon* 154 (2019) 67-73.
- [36] A.A. Voevodin, J.S. Zabinski, Nanocomposite and nanostructured tribological materials for space applications, *Composites Science and Technology* 65(5) (2005) 741-748.
- [37] H. Li, J. Wang, S. Gao, Q. Chen, L. Peng, K. Liu, X. Wei, Superlubricity between MoS₂ Monolayers, *Advanced Materials* 29(27) (2017) 1701474.
- [38] P. Wu, X. Li, C. Zhang, X. Chen, S. Lin, H. Sun, C.-T. Lin, H. Zhu, J. Luo, Self-Assembled Graphene Film as Low Friction Solid Lubricant in Macroscale Contact, *ACS Applied Materials & Interfaces* 9(25) (2017) 21554-21562.
- [39] M.R. Vazirisereshk, K. Hasz, M.-Q. Zhao, A.T.C. Johnson, R.W. Carpick, A. Martini, Nanoscale Friction Behavior of Transition-Metal Dichalcogenides: Role of the Chalcogenide, *ACS Nano* 14(11) (2020) 16013-16021.
- [40] M.R. Vazirisereshk, K. Hasz, R.W. Carpick, A. Martini, Friction Anisotropy of MoS₂: Effect of Tip-Sample Contact Quality, *The Journal of Physical Chemistry Letters* 11(16) (2020) 6900-6906.
- [41] M.R. Vazirisereshk, H. Ye, Z. Ye, A. Otero-de-la-Roza, M.-Q. Zhao, Z. Gao, A.T.C. Johnson, E.R. Johnson, R.W. Carpick, A. Martini, Origin of Nanoscale Friction Contrast between Supported Graphene, MoS₂, and a Graphene/MoS₂ Heterostructure, *Nano Letters* 19(8) (2019) 5496-5505.
- [42] S. Bhowmick, A. Banerji, A.T. Alpas, Role of humidity in reducing sliding friction of multilayered graphene, *Carbon* 87 (2015) 374-384.
- [43] C. Muratore, A.A. Voevodin, Chameleon Coatings: Adaptive Surfaces to Reduce Friction and Wear in Extreme Environments, *Annual Review of Materials Research* 39(1) (2009) 297-324.
- [44] J.M. Martin, C. Donnet, T. Le Mogne, T. Epicier, Superlubricity of molybdenum disulphide, *Physical Review B* 48(14) (1993) 10583-10586.
- [45] Z. Yang, S. Bhowmick, F.G. Sen, A.T. Alpas, Microscopic and atomistic mechanisms of sliding friction of MoS₂: Effects of undissociated and dissociated H₂O, *Applied Surface Science* 563 (2021) 150270.
- [46] Q. Xu, J. Zhang, X. Li, D.M. van Duin, Y. Hu, A.C.T. van Duin, T. Ma, How Polytetrafluoroethylene Lubricates Iron: An Atomistic View by Reactive Molecular Dynamics, *ACS Applied Materials & Interfaces* 14(4) (2022) 6239-6250.
- [47] G. De-Li, Z. Bing, X. Qun-Ji, W. Hong-Li, Effect of tribochemical reaction of polytetrafluoroethylene transferred film with substrates on its wear behaviour, *Wear* 137(2) (1990) 267-273.
- [48] T.F. Babuska, J.F. Curry, M.T. Dugger, P. Lu, Y. Xin, S. Klueter, A.C. Kozen, T. Grejtak, B.A. Krick, Role of Environment on the Shear-Induced Structural Evolution of MoS₂ and Impact on Oxidation and Tribological Properties for Space Applications, *ACS Applied Materials & Interfaces* 14(11) (2022) 13914-13924.
- [49] P. Najmi, N. Keshmiri, M. Ramezanzadeh, B. Ramezanzadeh, M. Arjmand, Epoxy nanocomposites holding molybdenum disulfide decorated with covalent organic framework: All-in-one coatings featuring thermal, UV-shielding, and mechanical properties, *Composites Part B: Engineering* 260 (2023) 110785.
- [50] J. Li, X. Ge, J. Luo, Random occurrence of macroscale superlubricity of graphite enabled by tribo-transfer of multilayer graphene nanoflakes, *Carbon* 138 (2018) 154-160.

- [51] D. Berman, A. Erdemir, A.V. Sumant, Few layer graphene to reduce wear and friction on sliding steel surfaces, *Carbon* 54 (2013) 454-459.
- [52] A. Macknojjia, A. Ayyagari, D. Zambrano, A. Rosenkranz, E.V. Shevchenko, D. Berman, Macroscale Superlubricity Induced by MXene/MoS₂ Nanocomposites on Rough Steel Surfaces under High Contact Stresses, *ACS Nano* 17(3) (2023) 2421–2430.
- [53] K. Yu, Y. Peng, H. Lang, S. Ding, Y. Huang, Material transfer mechanism for fabrication of superlubricity interface by reciprocating rubbing on graphite under high contact stress, *Carbon* 188 (2022) 420-430.
- [54] X. Zeng, Y. Peng, M. Yu, H. Lang, X.a. Cao, K. Zou, Dynamic Sliding Enhancement on the Friction and Adhesion of Graphene, Graphene Oxide, and Fluorinated Graphene, *ACS Applied Materials & Interfaces* 10(9) (2018) 8214-8224.
- [55] J.H. Chu, L.B. Tong, J.B. Zhang, S. Kamado, Z.H. Jiang, H.J. Zhang, G.X. Sun, Bio-inspired graphene-based coatings on Mg alloy surfaces and their integrations of anti-corrosive/wearable performances, *Carbon* 141 (2019) 154-168.
- [56] L.-F. Wang, T.-B. Ma, Y.-Z. Hu, H. Wang, Atomic-scale friction in graphene oxide: An interfacial interaction perspective from first-principles calculations, *Physical Review B* 86(12) (2012) 125436.
- [57] L.-F. Wang, T.-B. Ma, Y.-Z. Hu, H. Wang, T.-M. Shao, Ab Initio Study of the Friction Mechanism of Fluorographene and Graphane, *The Journal of Physical Chemistry C* 117(24) (2013) 12520-12525.
- [58] Z. He, Y. Zhu, H. Wu, Edge effect on interlayer shear in multilayer two-dimensional material assemblies, *International Journal of Solids and Structures* 204-205 (2020) 128-137.
- [59] L.-F. Wang, T.-B. Ma, Y.-Z. Hu, Q. Zheng, H. Wang, J. Luo, Superlubricity of two-dimensional fluorographene/MoS₂ heterostructure: a first-principles study, *Nanotechnology* 25(38) (2014) 385701.
- [60] Y. Sun, Y. Wang, E. Wang, B. Wang, H. Zhao, Y. Zeng, Q. Zhang, Y. Wu, L. Gu, X. Li, K. Liu, Determining the interlayer shearing in twisted bilayer MoS₂ by nanoindentation, *Nature Communications* 13(1) (2022) 3898.
- [61] G. Wang, Z. Dai, Y. Wang, P. Tan, L. Liu, Z. Xu, Y. Wei, R. Huang, Z. Zhang, Measuring Interlayer Shear Stress in Bilayer Graphene, *Physical Review Letters* 119(3) (2017) 036101.
- [62] J.R. Lince, Tribology of Co-sputtered Nanocomposite Au/MoS₂ Solid Lubricant Films over a Wide Contact Stress Range, *Tribology Letters* 17(3) (2004) 419-428.
- [63] I.L. Singer, R.N. Bolster, J. Wegand, S. Fayeulle, B.C. Stupp, Hertzian stress contribution to low friction behavior of thin MoS₂ coatings, *Appl. Phys. Lett.* 57(10) (1990) 995-997.
- [64] A.M. Couto Carneiro, R. Pinto Carvalho, F.M. Andrade Pires, Representative contact element size determination for micromechanical contact analysis of self-affine topographies, *International Journal of Solids and Structures* 206 (2020) 262-281.
- [65] A. Aymard, E. Delplanque, D. Dalmas, J. Scheibert, Designing metainterfaces with specified friction laws, *Science* 383(6679) (2024) 200-204.
- [66] V. Slesarenko, L. Pastewka, The bumpy road to friction control, *Science* 383(6679) (2024) 150-151.
- [67] Z. Deng, A. Smolyanitsky, Q. Li, X.-Q. Feng, R.J. Cannara, Adhesion-dependent negative friction coefficient on chemically modified graphite at the nanoscale, *Nature Materials* 11(12) (2012) 1032-1037.
- [68] J. Sun, Y. Zhang, Z. Lu, Q. Li, Q. Xue, S. Du, J. Pu, L. Wang, Superlubricity Enabled by Pressure-Induced Friction Collapse, *The Journal of Physical Chemistry Letters* 9(10) (2018) 2554-2559.
- [69] S. Ren, M. Cui, A. Martini, Y. Shi, H. Wang, J. Pu, Q. Li, Q. Xue, L. Wang, Macroscale superlubricity enabled by rationally designed MoS₂-based superlattice films, *Cell Reports Physical Science* 4(5) (2023) 101390.

[70] C. Dong, D. Jiang, Y. Fu, D. Wang, Q. Wang, L. Weng, M. Hu, X. Gao, J. Sun, Macro-superlubricity in sputtered MoS₂-based films by decreasing edge pinning effect, *Friction* 12(1) (2024) 52-63.

[71] Y. Shi, J. Zhang, J. Pu, S. Ren, H. Wang, X. Fan, T. Ma, L. Wang, Robust macroscale superlubricity enabled by tribo-induced structure evolution of MoS₂/metal superlattice coating, *Composites Part B: Engineering* 250 (2023) 110460.